AGU ADVANCING EARTH AND SPACE SCIENCES

Geophysical Research Letters

RESEARCH LETTER
10.1029/2025GL115061

Effective Heat Capacity and Its Role in Arctic Amplification

Michael Previdi[1] and Lorenzo M. Polvani[1,2,3]

[1]Lamont-Doherty Earth Observatory of Columbia University, Palisades, NY, USA, [2]Department of Applied Physics and Applied Mathematics, Columbia University, New York, NY, USA, [3]Department of Earth and Environmental Sciences, Columbia University, New York, NY, USA

Key Points:

- Arctic amplification develops rapidly following a CO_2 increase due to the Arctic's lower effective heat capacity compared to the tropics
- The Arctic's lower effective heat capacity is due to the presence of sea ice
- Because of the Arctic's lower effective heat capacity, CO_2 radiative forcing alone produces polar-amplified warming

Correspondence to:
M. Previdi,
mprevidi@ldeo.columbia.edu

Citation:
Previdi, M., & Polvani, L. M. (2025). Effective heat capacity and its role in Arctic amplification. *Geophysical Research Letters*, *52*, e2025GL115061. https://doi.org/10.1029/2025GL115061

Received 27 JAN 2025
Accepted 17 MAY 2025

Abstract Arctic amplification (AA), referring to the greater warming of the Arctic relative to lower latitudes, is a robust feature in observations and in climate model simulations driven by increasing greenhouse gases. In this study, we examine the rapid development of AA following abrupt CO_2 quadrupling in CMIP5 and CMIP6 models. We show that this rapid development of AA is a consequence of the Arctic's lower effective heat capacity compared to the tropics and global mean. The Arctic's lower heat capacity, which is due to the presence of sea ice, leads to polar-amplified warming in response to CO_2 radiative forcing alone. However, the full magnitude of AA can only be understood by also considering the feedbacks and energy transport changes that act to preferentially warm the Arctic region.

Plain Language Summary When atmospheric CO_2 is increased, the Arctic region warms faster than the rest of the planet, a phenomenon known as Arctic amplification (AA). AA is thought to occur as a result of several different processes, most importantly the loss of Arctic sea ice. Here, using climate model simulations driven by increased CO_2, we show that the very presence of sea ice in the Arctic is important for AA for a different reason: it causes the heat capacity of the Arctic climate system to be lower than for the planet as a whole. Because of its lower heat capacity, the Arctic warms up faster than the rest of the world when CO_2 is increased. Our results shed new insight into the underlying causes of AA.

1. Introduction

The greater warming of the Arctic relative to lower latitudes—known as Arctic amplification (AA)—is a robust response to increasing greenhouse gases, being evident in observations of recent climate change (Chylek et al., 2022; Gulev et al., 2021; Rantanen et al., 2022), and in future twenty-first century projections from climate models (Lee et al., 2021). AA has important impacts on a range of human and natural systems, both within and outside the Arctic, and understanding its underlying causes has been a long-standing challenge in climate dynamics (e.g., Previdi et al., 2021).

Recent work (Janoski et al., 2023; Previdi et al., 2020) has demonstrated that AA develops very rapidly in climate model simulations following an abrupt quadrupling of atmospheric CO_2 ($4 \times CO_2$). This rapid development of AA is illustrated in Figure 1a in $4 \times CO_2$ simulations from Coupled Model Intercomparison Project phases 5 and 6 (CMIP5 and CMIP6) climate models. In the first year of the model simulations, AA is already evident, with the multimodel mean Arctic warming of 2.4 K greatly exceeding the tropical warming of 1.0 K. After the first decade of the simulations, the Arctic warming has reached 8.1 K, again much greater than the tropical warming of 3.2 K. Following this period of rapid warming, both Arctic and tropical temperatures increase at a much slower rate for the remainder of the 150-year simulations.

Previous studies attempting to identify the physical mechanisms underlying AA have often assessed the differences in perturbation energy fluxes between the Arctic and lower latitudes (e.g., Goosse et al., 2018; Hahn et al., 2021; Janoski et al., 2023; Pithan & Mauritsen, 2014; Previdi et al., 2020). Within this framework, a particular mechanism (e.g., CO_2 forcing, feedback, or energy transport change) is viewed as contributing to AA if it produces a larger perturbation energy flux (in W m^{-2}) in the Arctic than in the tropics (or global mean). We show here that energy flux considerations alone are insufficient to understand the rapid development of AA shown in Figure 1a, and that this feature can only be understood by also considering the lower effective heat capacity of the Arctic climate system compared to the tropics. This lower Arctic heat capacity, we will show, has the important implication that CO_2 forcing alone produces polar-amplified warming.

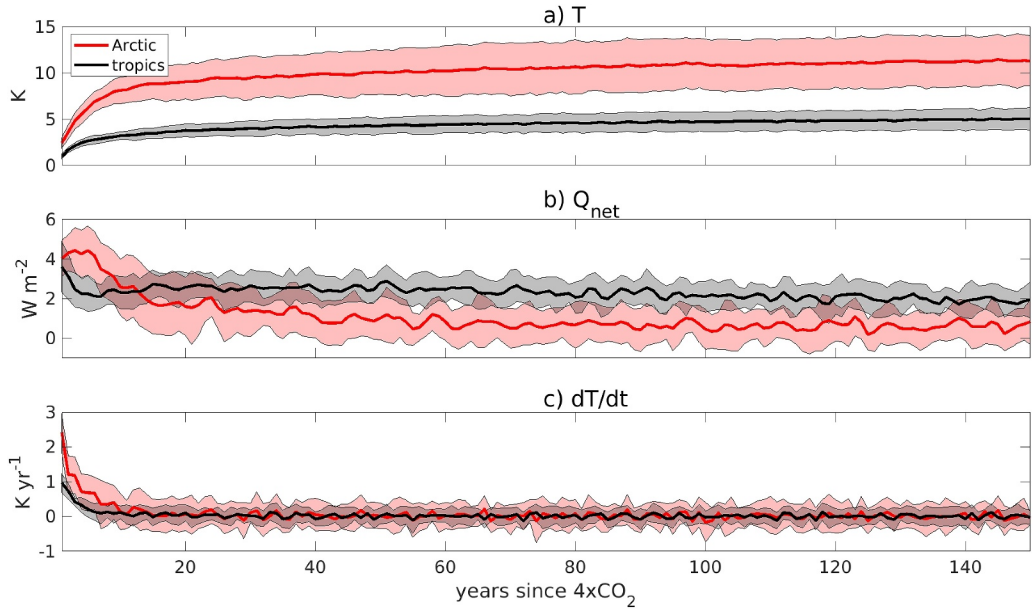

Figure 1. Time series of annual-mean (a) surface air temperature (SAT) response, (b) net heat uptake, and (c) warming rate averaged over the Arctic (60°N–90°N) and tropics (30°S–30°N). The SAT response and net heat uptake are computed as the difference between the abrupt $4 \times CO_2$ simulation and the 30-year climatology of the piControl simulation. The warming rate dT/dt (panel (c)) is computed by differentiating the SAT response (panel (a)) using a backward finite difference approximation. Lines represent multimodel means and shading represents the plus/minus 1 standard deviation spread.

2. Methods

2.1. Climate Model Output

We analyze climate model simulations in which the atmospheric CO_2 concentration is instantaneously quadrupled relative to pre-industrial levels. These abrupt $4 \times CO_2$ simulations are analyzed for 5 CMIP5 models (CanESM2, IPSL-CM5A-LR, MPI-ESM-LR, MRI-CGCM3, and NorESM1-M) and 13 CMIP6 models (ACCESS-CM2, ACCESS-ESM1-5, CanESM5, CESM2, CNRM-CM6-1, CNRM-ESM2-1, GFDL-ESM4, GISS-E2-1-G, IPSL-CM6A-LR, MIROC6, MPI-ESM1-2-LR, NorESM2-LM, and NorESM2-MM). These are the models that provided all of the necessary output for our analysis. We average the results from all 18 models together when computing multimodel means.

For each model, we employ two abrupt $4 \times CO_2$ simulations: a fully coupled simulation, and a fixed sea surface temperature (SST) simulation in which the SST and sea-ice concentration (SIC) are held fixed at pre-industrial levels. Each of these abrupt $4 \times CO_2$ simulations has a corresponding pre-industrial control (piControl) simulation with pre-industrial atmospheric CO_2 levels. We compute climate responses to increased CO_2 as the difference between the abrupt $4 \times CO_2$ simulation and the 30-year climatology of its corresponding piControl simulation.

2.2. Energy Budget Framework

We begin by considering the following relationship between effective heat capacity C_{eff}, surface air temperature (SAT) change, and heat uptake:

$$C_{\text{eff}} \frac{\mathrm{d}T}{\mathrm{d}t} = Q_{\text{net}} \tag{1}$$

where dT/dt is the time rate of change of the SAT response and Q_{net} is the net heat uptake of the atmosphere-ocean column. We take Q_{net} to be the combination of ocean heat uptake and sea-ice volume (SIV) loss, that is,

$$Q_{\text{net}} = \Delta \frac{\mathrm{dOHC}}{\mathrm{d}t} - \Delta \frac{\mathrm{dSIV}}{\mathrm{d}t} \tag{2}$$

where dOHC/dt and dSIV/dt are the time rates of change of the vertically integrated ocean heat content and the SIV, respectively, and Δ represents the response to $4 \times CO_2$. We neglect heat uptake by the atmosphere and land surface, which is negligible on the annual and longer timescales we focus on. The effective heat capacity C_{eff} is computed as the ratio of Q_{net} to dT/dt (Equation 1). C_{eff} is determined by the portion of the atmosphere-ocean column interacting with a heating perturbation at a given time. In the early years (e.g., the first decade) following $4 \times CO_2$, heat uptake is mostly confined to the ocean mixed layer, and thus C_{eff} is similar to the mixed layer heat capacity (see Section 3.1). On longer timescales, C_{eff} increases as the $4 \times CO_2$ heating perturbation penetrates to greater ocean depths.

Q_{net} can also be expressed as

$$Q_{\text{net}} = \Delta R + \Delta \text{AHT} + \Delta \text{OHT} \tag{3}$$

where R is the net downward top-of-atmosphere (TOA) radiation, AHT is the convergence of the atmospheric heat transport, and OHT is the convergence of the ocean heat transport. We compute AHT as the difference between the net downward energy fluxes at the surface and TOA, thus neglecting atmospheric energy storage which is negligible on annual and longer timescales. ΔOHT is computed as the residual in Equation 3.

We further decompose ΔR as

$$\Delta R = \Delta R_{\text{CO2}} + \Delta R_P + \Delta R_{\text{LR}} + \Delta R_{\text{WV}} + \Delta R_{\text{Alb}} + \Delta R_{\text{Cld}} \tag{4}$$

where the terms on the right-hand side of the equation represent, from left to right, the TOA radiation changes due to the $4 \times CO_2$ forcing, the Planck response (P) associated with vertically uniform warming, and changes in the tropospheric lapse rate (LR), water vapor (WV), surface albedo (Alb), and clouds (Cld). We take ΔR_{CO2} to be the effective radiative forcing (ERF) from $4 \times CO_2$, computed as the change in the net TOA radiation in the fixed SST simulations. The remaining terms on the right-hand side of Equation 4, with the exception of ΔR_{Cld}, are computed using the radiative kernel method (Soden et al., 2008), employing kernels from the CESM-CAM5 climate model (Pendergrass et al., 2018). ΔR_{Cld} is computed as the residual in Equation 4.

Recognizing that the ERF computed from the fixed SST simulations (i.e., ΔR_{CO2}) includes the effects of the land (and sea ice) surface temperature adjustment to $4 \times CO_2$, we perform an alternate ERF calculation to remove these effects (see Forster et al., 2021):

$$\Delta R_{\text{CO2 (alt)}} = \Delta R_{\text{CO2}} - k\Delta \text{Ts}_{\text{Adj}} \tag{5}$$

where k is the CESM-CAM5 surface temperature radiative kernel, and $\Delta \text{Ts}_{\text{Adj}}$ is the surface temperature change (adjustment) in the fixed SST simulations. Note that all terms in Equations 1–5 have units of W m^{-2}.

In order to compute ΔR_P, ΔR_{LR}, ΔR_{WV}, and ΔR_{Alb} using the radiative kernel method, we first separate the total (Tot) response to $4 \times CO_2$ into adjustment (Adj) and feedback (Fdbk):

$$\Delta x_{\text{Tot}} = \Delta x_{\text{Adj}} + \Delta x_{\text{Fdbk}} \tag{6}$$

where Δx represents the response of atmospheric or surface temperature, WV, or surface albedo. We compute Δx_{Tot} as the difference between the fully coupled abrupt $4 \times CO_2$ and piControl simulations, Δx_{Adj} as the difference between the corresponding fixed SST simulations, and Δx_{Fdbk} as Δx_{Tot} minus Δx_{Adj}. We then multiply Δx_{Fdbk} by the radiative kernel to compute the temperature, WV and surface albedo feedbacks (i.e., ΔR_P, ΔR_{LR}, ΔR_{WV}, and ΔR_{Alb}). This approach thus ensures that the computed feedbacks do not include the effects of Δx_{Adj}, since the latter are already included in the ERF (i.e., ΔR_{CO2}).

Having decomposed Q_{net} as in Equations 3 and 4, we next decompose dT/dt by dividing each component of Q_{net} by C_{eff} (Equation 1). We consider mean SAT and energy budget responses averaged over the Arctic, tropical and global domains. Unless indicated otherwise, Arctic means represent the area-weighted average over 60°N–90°N. Tropical and global means represent the area-weighted average over 30°S–30°N and 90°S–90°N, respectively.

Table 1
Net Heat Uptake (Q_{net}), Warming Rate (dT/dt), and Effective Heat Capacity (C_{eff}) for the Arctic, Tropical, and Global Domains Averaged Over the First Decade of the Model Simulations

	Q_{net} (W m^{-2})	dT/dt (K yr^{-1})	C_{eff} (W m^{-2} K^{-1} yr)
Arctic (60°N–90°N)	3.8 ± 1.2	0.81 ± 0.54	4.7 ± 0.9
Arctic (70°N–90°N)	5.1 ± 1.7	0.96 ± 0.69	5.4 ± 1.2
Tropics (30°S–30°N)	2.5 ± 0.9	0.32 ± 0.23	7.9 ± 2.1
Global (90°S–90°N)	4.1 ± 0.6	0.35 ± 0.15	11.6 ± 1.4

Note. Values shown are multimodel means ±1 standard deviation.

3. Results

3.1. Effective Heat Capacity of the Arctic and Tropical Climate Systems

We now return our attention to the rapid development of AA following $4 \times CO_2$. Our analysis focuses herein mostly on the first decade of the model simulations, the period of most rapid warming (Figure 1a). Averaged over this first decade, the Arctic mean Q_{net} (3.8 ± 1.2 W m^{-2}) is 52% larger than the tropical mean Q_{net} (2.5 ± 0.9 W m^{-2}; Figure 1b and Table 1), which, we will show, is due primarily to stronger positive feedbacks over the Arctic (see Section 3.2). The majority (87%, or 3.3 W m^{-2}) of the Arctic mean Q_{net} is associated with ocean heat uptake (i.e., ΔdOHC/dt), with the remaining fraction (13%, or 0.5 W m^{-2}) due to SIV loss (i.e., ΔdSIV/dt, Equation 2).

If the effective heat capacity of the Arctic and tropical climate systems was the same, one would expect that dT/dt averaged over the first decade of the model simulations would also be 52% larger in the Arctic than in the tropics (as for Q_{net}, see Equation 1). However, we find that the Arctic mean dT/dt (0.81 ± 0.54 K yr^{-1}) is actually ∼2.5 times (150%) larger than the tropical mean dT/dt (0.32 ± 0.23 K yr^{-1}, Figure 1c and Table 1), implying a lower effective heat capacity of the Arctic compared to the tropics. This lower Arctic heat capacity is also suggested by the Q_{net} time series shown in Figure 1b. After the first decade of the model simulations, the multimodel mean Arctic Q_{net} quickly falls below the tropical Q_{net} and remains there for the duration of the simulations. In a handful of individual models, the Arctic Q_{net} returns to zero a few decades following $4 \times CO_2$ (not shown), indicating a return to equilibrium. In contrast, the multimodel mean tropical Q_{net} remains relatively constant, with no individual models returning to equilibrium during the 150-year simulations. The faster return to equilibrium of the Arctic climate system following $4 \times CO_2$ is another indication of its lower effective heat capacity.

We estimate C_{eff} for the first decade of the simulations by computing the year 1–10 average values of Q_{net} and dT/dt and then taking their ratio (Equation 1). This yields a multimodel mean C_{eff} for the tropics (7.9 ± 2.1 W m^{-2} K^{-1} yr) that is 68% larger than that for the Arctic (4.7 ± 0.9 W m^{-2} K^{-1} yr, Table 1), a difference that is highly significant ($p < 0.001$) based on a t-test. For comparison, we estimate the global C_{eff} to be 11.6 ± 1.4 W m^{-2} K^{-1} yr (Table 1). This agrees well with previous studies (Dickinson, 1981; Geoffroy et al., 2013) that found a global C_{eff} of the order 10 W m^{-2} K^{-1} yr for the ocean mixed layer, suggesting that most of the heat uptake in the first decade of our simulations is occurring within the mixed layer. After the first decade, C_{eff} increases as the $4 \times CO_2$ heating perturbation penetrates to greater ocean depths, with C_{eff} for the deep ocean estimated to be of order 100 W m^{-2} K^{-1} yr (Dickinson, 1981; Geoffroy et al., 2013).

Our results lead naturally to the following question: what factors are responsible for the Arctic's low effective heat capacity? To answer this, we examine the spatial pattern of C_{eff} over the Arctic for the first decade of the simulations (Figure 2). It is immediately evident that the largest values of C_{eff} occur equatorward of the sea-ice edge (cyan contour) over open ocean, with local C_{eff} maxima in the Labrador and Norwegian Seas likely coinciding with areas of deep water formation. In contrast, sea ice-covered areas are generally characterized by much smaller C_{eff}. Over much of the ice-covered ocean, C_{eff} is less than 5 W m^{-2} K^{-1} yr, which is more similar to land (assumed zero heat capacity and masked out in Figure 2) than to the open ocean, high C_{eff} areas to the south.

These results therefore suggest that the presence of sea ice may explain the Arctic's lower effective heat capacity compared to the tropics. Another consideration, however, is whether C_{eff} differences between the Arctic and tropics may also be due to differences in the relative fractions of land versus ocean. The land area fraction for the Arctic (60°N–90°N) domain is 52%, compared to 26% for the tropics (30°S–30°N). Is this greater abundance of low heat capacity land in the Arctic the reason for the Arctic's lower C_{eff}? To test this possibility, we recomputed C_{eff} using an alternative definition for the Arctic, 70°N–90°N. When defined this way, the Arctic has a land area fraction of 27%, thus nearly identical to that of the tropics. Despite this, the Arctic's effective heat capacity (5.4 ± 1.2 W m^{-2} K^{-1} yr) remains significantly lower than that of the tropics (7.9 ± 2.1 W m^{-2} K^{-1} yr, see Table 1). This result is therefore robust to how one chooses to define the Arctic region.

We conclude then that it is the presence of sea ice in the Arctic climate system that explains the Arctic's lower value of C_{eff} compared to the tropics. Sea ice acts as an effective barrier between the atmosphere and ocean, thus limiting ocean heat uptake (ΔdOHC/dt) and allowing for a rapid warming of the SAT following $4 \times CO_2$, akin to what occurs over land. While sea ice melt (ΔdSIV/dt) does contribute to the Arctic mean Q_{net} (and thus to C_{eff}), as

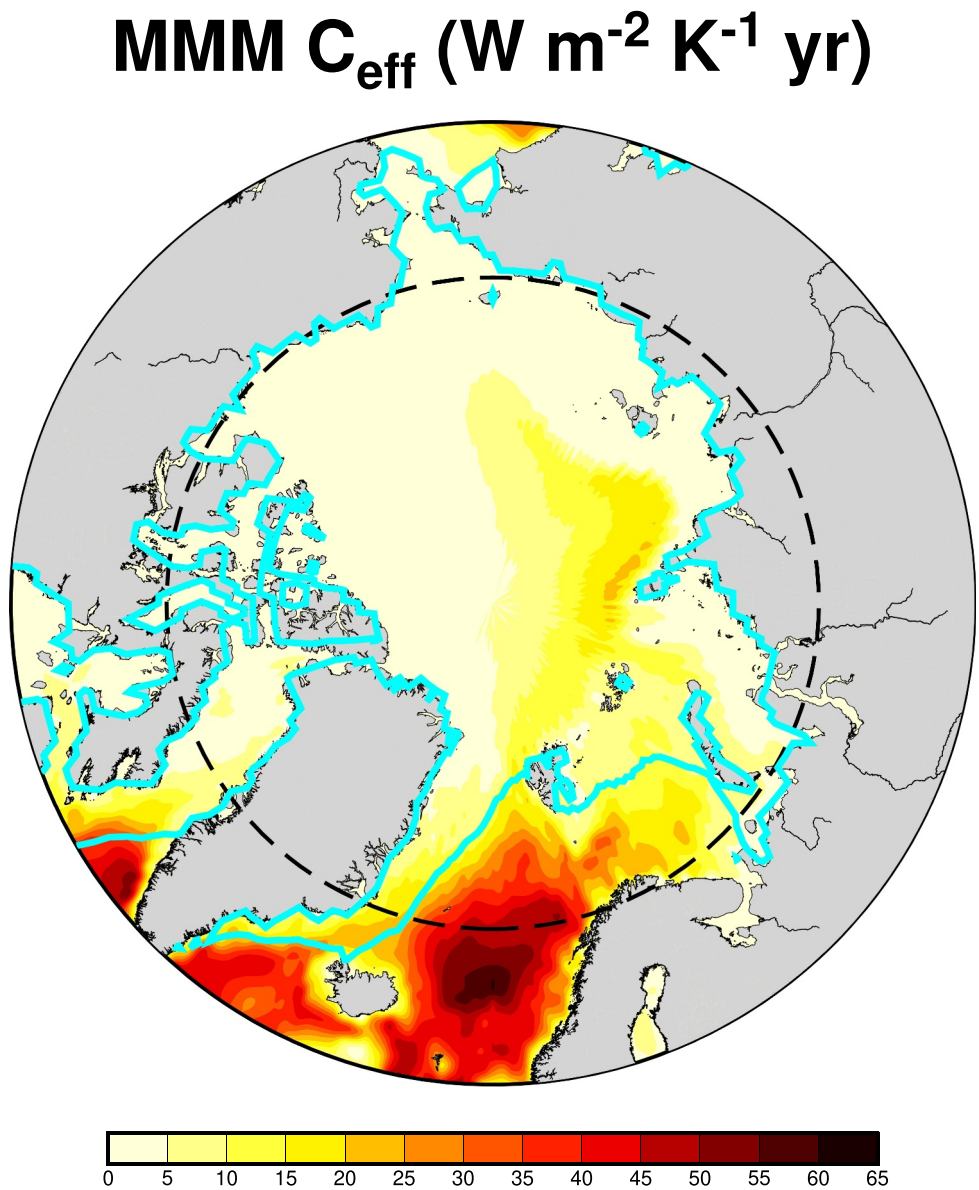

Figure 2. Multimodel mean (MMM) effective heat capacity (C_{eff}), computed as the ratio of the year 1–10 average values of net heat uptake (Q_{net}) and warming rate (dT/dt; see Equation 1). C_{eff} is plotted for the region poleward of 60°N, with the dashed black contour marking the 70°N parallel. The cyan contour represents the MMM sea-ice edge, defined as 15% sea-ice concentration.

noted above, this is a far smaller heat reservoir than the potential ocean heat reservoir underlying the sea ice. In other words, the limitation of ocean heat uptake by sea ice outweighs the Q_{net} contribution from sea ice melt, resulting in the Arctic's effective heat capacity being lower with sea ice present than without it. In the next section, we will further explore the implications of the C_{eff} difference between the Arctic and tropics for polar-amplified warming.

3.2. Contributions to Polar-Amplified Warming

As discussed in Section 1, a common approach that is used to identify the physical mechanisms contributing to AA is to assess the differences in perturbation energy fluxes between the Arctic and lower latitudes (e.g., Goosse et al., 2018; Hahn et al., 2021; Janoski et al., 2023; Pithan & Mauritsen, 2014; Previdi et al., 2020). This involves decomposing Q_{net} into contributions from CO_2 forcing, climate feedbacks, and energy transport changes (see

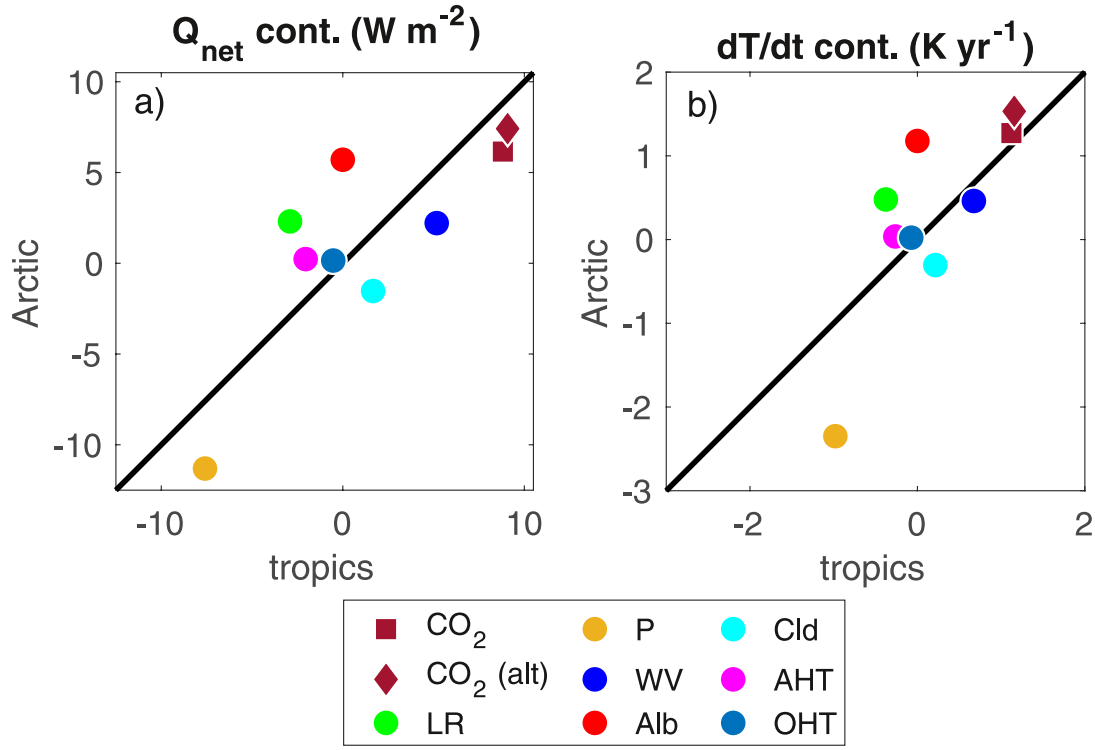

Figure 3. Multimodel mean contributions (cont.) to (a) net heat uptake (Q_{net}) and (b) total warming rate (dT/dt) averaged over the first decade of the model simulations and over the Arctic (60°N–90°N) and tropics (30°S–30°N). Decomposition of Q_{net} (panel (a)) follows Equations 3 and 4, with each component of Q_{net} divided by C_{eff} to obtain contributions to dT/dt (panel (b)). The diamond (CO_2 (alt)) and square (CO_2) symbols denote the $4 \times CO_2$ effective radiative forcing with and without the effects of the surface temperature adjustment removed, respectively (see Section 2.2 and Equation 5). The black line in each panel represents the 1:1 line.

Equations 3 and 4), and then comparing each contribution in the Arctic and tropics (or global mean). We present such a Q_{net} decomposition for the first decade of our model simulations in Figure 3a. Individual components of Q_{net} (colored symbols) that lie above the 1:1 line are viewed, in this framework, as contributing to AA, whereas Q_{net} components lying below the 1:1 line are viewed as opposing AA (and contributing to tropical amplification of warming).

Figure 3a thus suggests that the surface albedo feedback, LR feedback, and AHT response contribute to AA, whereas the CO_2 forcing, WV feedback, and cloud feedback oppose AA, in agreement with previous studies (Goosse et al., 2018; Hahn et al., 2021; Pithan & Mauritsen, 2014). These previous studies analyzed the atmospheric energy budget alone, which does not include an OHT term. In our analysis of the energy budget of the whole atmosphere-ocean column, the OHT term lies slightly above the 1:1 line (Figure 3a), suggesting that it weakly contributes to AA. Finally, previous studies (e.g., Goosse et al., 2018; Hahn et al., 2021; Janoski et al., 2023; Pithan & Mauritsen, 2014; Previdi et al., 2020) have often defined the Planck response to be the local deviation from the global mean. When defined in this way, this term contributes to AA, reflecting the fact that a larger temperature change is needed in the colder Arctic than in the warmer tropics to balance a given perturbation energy flux through a change in outgoing longwave radiation (OLR). In contrast, we show in Figure 3a the total Planck response, which is more negative in the Arctic than in the tropics (thus opposing AA) since the greater Arctic warming leads to a larger increase in OLR.

Individual components of Q_{net} are often expressed as "warming contributions" (in K) by normalizing the perturbation energy fluxes (in W m^{-2}) by the magnitude of the (typically, global mean) Planck response (in W m^{-2} K^{-1}; e.g., see Goosse et al., 2018; Hahn et al., 2021; Janoski et al., 2023; Pithan & Mauritsen, 2014; Previdi et al., 2020). These warming contributions are interpreted as the temperature change required to balance a given perturbation energy flux through a change in OLR. While useful, they do not allow for an assessment of the transient warming *rate* (i.e., dT/dt), which depends on both Q_{net} and C_{eff} (see Equation 1). In Figure 3b, we

decompose dT/dt for the first decade of our model simulations into contributions from CO_2 forcing, climate feedbacks, and energy transport changes by normalizing the respective perturbation energy fluxes by the effective heat capacity.

Decomposing dT/dt (Figure 3b) rather than Q_{net} (Figure 3a) does not change the relative importance of the various energy budget terms for the warming in a particular region (i.e., Arctic or tropics). However, it can change the position of a given term relative to the 1:1 line, and thus the inferred importance of that term for AA. Most notably, in the traditional Q_{net}/warming contributions framework (Figure 3a), the CO_2 forcing (square and diamond symbols) lies below the 1:1 line, suggesting that it opposes AA. However, in the alternative dT/dt framework (Figure 3b), the CO_2 forcing lies above the 1:1 line, suggesting that it contributes to AA. The choice of one framework over the other should be guided by whether one wishes to understand the equilibrium or the transient warming. At equilibrium, the warming depends solely on the total perturbation energy flux due to the CO_2 forcing, climate feedbacks, and energy transport changes, and thus the traditional framework is an appropriate choice. In our analysis, however, we wish to understand the transient warming rate in the first decade of the model simulations, which depends on both Q_{net} and C_{eff}. In this case, the alternative framework (Figure 3b) is the superior choice, since it accounts for the difference in the effective heat capacity between the Arctic and tropical climate systems.

Our results therefore suggest that even though the CO_2 forcing (in W m^{-2}) is larger in the tropics than in the Arctic (Figure 3a), this forcing drives more rapid warming in the Arctic (Figure 3b) as a result of the Arctic's lower effective heat capacity. We note, however, that the multimodel mean CO_2-induced warming rate in the Arctic is 1.3 ± 0.2 K yr^{-1} (1.5 ± 0.3 K yr^{-1}), which is only 18% (25%) larger than the tropical CO_2-induced warming rate of 1.1 ± 0.3 K yr^{-1} (1.2 ± 0.3 K yr^{-1}). (Values outside and inside the parentheses represent the CO_2-induced warming rate computed using ΔR_{CO2} (square symbol in Figure 3) and $\Delta R_{CO2\ (alt)}$ (diamond symbol in Figure 3), respectively, with uncertainty ranges corresponding to ± 1 standard deviation across the models.) By comparison, the total Arctic warming rate (0.81 ± 0.54 K yr^{-1}) is ~2.5 times (150%) larger than the total tropical warming rate (0.32 ± 0.23 K yr^{-1}, see Table 1). Thus, while CO_2 forcing contributes to the rapid development of AA in the first decade of our model simulations, the full magnitude of AA can only be understood by also considering the other processes that act to preferentially warm the Arctic region: the surface albedo feedback, the LR feedback, and the AHT and OHT responses (Figure 3b).

4. Discussion and Conclusions

Previous work (Janoski et al., 2023; Previdi et al., 2020) has shown that AA develops rapidly (within the first year) in climate model simulations following an abrupt quadrupling of atmospheric CO_2. In the current study, we have demonstrated that this rapid development of AA is a consequence of the lower effective heat capacity of the Arctic climate system compared to the tropics and global mean. This lower Arctic heat capacity, in turn, is a consequence of sea ice cover at high northern latitudes. Sea ice effectively insulates the ocean from the atmosphere (e.g., Previdi et al., 2021; Serreze & Barry, 2011; Vihma, 2014), thus limiting ocean heat uptake and allowing for a rapid warming of the SAT following $4 \times CO_2$. This implies that as sea ice melts, the effective heat capacity of the Arctic climate system increases, contributing to reduced rates of Arctic warming. This mechanism has been invoked to explain the summertime minimum in Arctic warming and AA (Dwyer et al., 2012; Hahn et al., 2022; Manabe & Stouffer, 1980; Manabe et al., 1992; Mann & Park, 1996; Robock, 1983; Sejas & Taylor, 2023), which is a robust feature in both observations and in model simulations driven by increasing greenhouse gases. In contrast, in fall and winter, when the Arctic Ocean is a heat source for the atmosphere, diminished sea ice cover contributes to enhanced rates of Arctic warming by facilitating greater ocean-to-atmosphere heat exchange (e.g., Dai et al., 2019; Screen & Simmonds, 2010). Finally, in an annual-mean sense, weaker AA in future climate simulations with greatly diminished sea ice cover (e.g., Dai et al., 2019) may be partly due to higher Arctic C_{eff}, in addition to the loss/weakening of sea ice-related feedbacks.

Our results therefore suggest that the transient warming response to increased CO_2 in observations and model simulations will be characterized by AA, owing fundamentally to the Arctic's lower effective heat capacity compared to the tropics and global mean. We stress, however, that heat capacity differences between the Arctic and lower latitudes cannot explain the full magnitude of AA in transient warming scenarios, nor can they explain the persistence of AA in the equilibrium response. Understanding these aspects of AA requires additional consideration of the feedbacks and energy transport changes that act to preferentially warm the Arctic region.

Thus, effective heat capacity, while not the sole consideration, is an important factor explaining the basic existence of AA under transient CO_2-induced warming.

Conflict of Interest

The authors declare no conflicts of interest relevant to this study.

Data Availability Statement

The CMIP5 and CMIP6 model data can be obtained from the Earth System Grid Federation at https://aims2.llnl.gov/search/. The post-processed data and the analysis scripts are available under https://doi.org/10.5281/zenodo.13388534 (Previdi, 2025).

Acknowledgments
M. P. and L. M. P. are partially supported by a Grant from the National Science Foundation to Columbia University.

References

Chylek, P., Folland, C., Klett, J. D., Wang, M., Hengartner, N., Lesins, G., & Dubey, M. K. (2022). Annual mean Arctic Amplification 1970–2020: Observed and simulated by CMIP6 climate models. *Geophysical Research Letters*, *49*(13), e2022GL099371. https://doi.org/10.1029/2022gl099371

Dai, A., Luo, D., Song, M., & Liu, J. (2019). Arctic amplification is caused by sea-ice loss under increasing CO_2. *Nature Communications*, *10*(1), 121. https://doi.org/10.1038/s41467-018-07954-9

Dickinson, R. E. (1981). Convergence rate and stability of ocean-atmosphere coupling schemes with a zero-dimensional climate model. *Journal of the Atmospheric Sciences*, *38*(10), 2112–2120. https://doi.org/10.1175/1520-0469(1981)038<2112:crasoo>2.0.co;2

Dwyer, J. G., Biasutti, M., & Sobel, A. H. (2012). Projected changes in the seasonal cycle of surface temperature. *Journal of Climate*, *25*(18), 6359–6374. https://doi.org/10.1175/jcli-d-11-00741.1

Forster, P., Storelvmo, T., Armour, K., Collins, W., Dufresne, J.-L., Frame, D., et al. (2021). The Earth's energy budget, climate feedbacks, and climate sensitivity. In V. Masson-Delmotte, P. Zhai, A. Pirani, S. L. Connors, C. Péan, S. Berger, et al. (Eds.), *Climate change 2021: The physical science basis. Contribution of working group I to the sixth assessment report of the intergovernmental panel on climate change* (pp. 923–1054). Cambridge University Press.

Geoffroy, O., Saint-Martin, D., Olivié, D. J. L., Voldoire, A., Bellon, G., & Tytéca, S. (2013). Transient climate response in a two-layer energy-balance model. Part I: Analytical solution and parameter calibration using CMIP5 AOGCM experiments. *Journal of Climate*, *26*, 1841–1857.

Goosse, H., Kay, J. E., Armour, K. C., Bodas-Salcedo, A., Chepfer, H., Docquier, D., et al. (2018). Quantifying climate feedbacks in polar regions. *Nature Communications*, *9*(1), 1919. https://doi.org/10.1038/s41467-018-04173-0

Gulev, S. K., Thorne, P. W., Ahn, J., Dentener, F. J., Domingues, C. M., Gerland, S., et al. (2021). Changing state of the climate system. In V. Masson-Delmotte, P. Zhai, A. Pirani, S. L. Connors, C. Péan, S. Berger, et al. (Eds.), *Climate change 2021: The physical science basis. Contribution of working group I to the sixth assessment report of the intergovernmental panel on climate change* (pp. 287–422). Cambridge University Press.

Hahn, L. C., Armour, K. C., Battisti, D. S., Eisenman, I., & Bitz, C. M. (2022). Seasonality in Arctic warming driven by sea ice effective heat capacity. *Journal of Climate*, *35*(5), 1629–1642. https://doi.org/10.1175/jcli-d-21-0626.1

Hahn, L. C., Armour, K. C., Zelinka, M. D., Bitz, C. M., & Donohoe, A. (2021). Contributions to polar amplification in CMIP5 and CMIP6 models. *Frontiers in Earth Science*, *9*, 710036. https://doi.org/10.3389/feart.2021.710036

Janoski, T. P., Previdi, M., Chiodo, G., Smith, K. L., & Polvani, L. M. (2023). Ultrafast Arctic amplification and its governing mechanisms. *Environmental Research: Climate*, *2*(3), 035009. https://doi.org/10.1088/2752-5295/ace211

Lee, J.-Y., Marotzke, J., Bala, G., Cao, L., Corti, S., Dunne, J. P., et al. (2021). Future global climate: Scenario-based projections and near-term information. In V. Masson-Delmotte, P. Zhai, A. Pirani, S. L. Connors, C. Péan, S. Berger, et al. (Eds.), *Climate change 2021: The physical science basis. Contribution of working group I to the sixth assessment report of the intergovernmental panel on climate change* (pp. 553–672). Cambridge University Press.

Manabe, S., Spelman, M. J., & Stouffer, R. J. (1992). Transient responses of a coupled ocean–atmosphere model to gradual changes of atmospheric CO_2. Part II: Seasonal response. *Journal of Climate*, *5*(2), 105–126. https://doi.org/10.1175/1520-0442(1992)005<0105:troaco>2.0.co;2

Manabe, S., & Stouffer, R. J. (1980). Sensitivity of a global climate model to an increase of CO_2 concentration in the atmosphere. *Journal of Geophysical Research*, *85*(C10), 5529–5554. https://doi.org/10.1029/jc085ic10p05529

Mann, M. E., & Park, J. (1996). Greenhouse warming and changes in the seasonal cycle of temperature: Model versus observations. *Geophysical Research Letters*, *23*(10), 1111–1114. https://doi.org/10.1029/96gl01066

Pendergrass, A. G., Conley, A., & Vitt, F. M. (2018). Surface and top-of-atmosphere radiative feedback kernels for CESM-CAM5. *Earth System Science Data*, *10*(1), 317–324. https://doi.org/10.5194/essd-10-317-2018

Pithan, F., & Mauritsen, T. (2014). Arctic amplification dominated by temperature feedbacks in contemporary climate models. *Nature Geoscience*, *7*(3), 181–184. https://doi.org/10.1038/ngeo2071

Previdi, M. (2025). Data and analysis scripts for: "Effective heat capacity and its role in Arctic amplification" [Dataset]. https://doi.org/10.5281/zenodo.13388534

Previdi, M., Janoski, T. P., Chiodo, G., Smith, K. L., & Polvani, L. M. (2020). Arctic amplification: A rapid response to radiative forcing. *Geophysical Research Letters*, *47*(17), e2020GL089933. https://doi.org/10.1029/2020gl089933

Previdi, M., Smith, K. L., & Polvani, L. M. (2021). Arctic amplification of climate change: A review of underlying mechanisms. *Environmental Research Letters*, *16*(9), 093003. https://doi.org/10.1088/1748-9326/ac1c29

Rantanen, M., Karpechko, A. Y., Lipponen, A., Nordling, K., Hyvärinen, O., Ruosteenoja, K., et al. (2022). The Arctic has warmed nearly four times faster than the globe since 1979. *Communications Earth & Environment*, *3*(1), 168. https://doi.org/10.1038/s43247-022-00498-3

Robock, A. (1983). Ice and snow feedbacks and the latitudinal and seasonal distribution of climate sensitivity. *Journal of the Atmospheric Sciences*, *40*(4), 986–997. https://doi.org/10.1175/1520-0469(1983)040<0986:iasfat>2.0.co;2

Screen, J. A., & Simmonds, I. (2010). Increasing fall-winter energy loss from the Arctic Ocean and its role in Arctic temperature amplification. *Geophysical Research Letters*, *37*(16), L16707. https://doi.org/10.1029/2010gl044136

Sejas, S. A., & Taylor, P. C. (2023). The role of sea ice in establishing the seasonal Arctic warming pattern. *Environmental Research: Climate*, *2*(3), 035008. https://doi.org/10.1088/2752-5295/ace20f

Serreze, M. C., & Barry, R. G. (2011). Processes and impacts of Arctic amplification: A research synthesis. *Global and Planetary Change*, *77*(1–2), 85–96. https://doi.org/10.1016/j.gloplacha.2011.03.004

Soden, B. J., Held, I. M., Colman, R., Shell, K. M., Kiehl, J. T., & Shields, C. A. (2008). Quantifying climate feedbacks using radiative kernels. *Journal of Climate*, *21*(14), 3504–3520. https://doi.org/10.1175/2007jcli2110.1

Vihma, T. (2014). Effects of Arctic sea ice decline on weather and climate: A review. *Surveys in Geophysics*, *35*(5), 1175–1214. https://doi.org/10.1007/s10712-014-9284-0